

# Enabling visible-light absorption and $p$ -type doping in $\text{In}_2\text{O}_3$ by adding Bi

Fernando P. Sabino<sup>1</sup>, Su-Huai Wei<sup>2</sup>, Anderson Janotti<sup>1</sup>

<sup>1</sup>*Department of Materials Science and Engineering,*

*University of Delaware, Newark, Delaware 19716, USA and*

<sup>2</sup>*Beijing Computational Science Research Center, Beijing 100094, China*

$\text{In}_2\text{O}_3$  is a prototype wide-band-gap semiconductor that exhibits metallic conductivity when highly doped with Sn while retaining a high degree of transparency to visible light. It is widely used as a transparent window/electrode in solar cells and LEDs. The functionality of  $\text{In}_2\text{O}_3$  would be greatly extended if  $p$ -type conductivity could also be achieved. Using electronic structure calculations, we show that adding Bi to  $\text{In}_2\text{O}_3$ , in the form of dilute  $(\text{In}_{1-x}\text{Bi}_x)_2\text{O}_3$  alloys, leads to a new valence band that is sufficiently higher in energy than the original O- $2p$  valence band to allow for  $p$ -type doping. Moreover, the raised valence band in the  $(\text{In}_{1-x}\text{Bi}_x)_2\text{O}_3$  dilute alloys leads to strong optical absorption in the visible spectrum, opening up for new applications such as a wide band gap absorber layer in tandem solar cells.

Keywords: Indium bismuth oxide, band gap tuning, high optical absorption

$\text{In}_2\text{O}_3$  is a wide-band-gap material, extensively used as a transparent conducting oxide. When heavily doped with Sn, often called ITO, it displays electrical conductivities around  $1 \times 10^3 \text{ S cm}^{-1}$ , while preserving a high transparency to visible light [1, 2]. The combination of optical transparency and high electrical conductivity is desirable for many device applications such as liquid-crystal displays, OLEDs, touchscreens, and transparent contacts in photovoltaic devices [3–6]. The functionality of  $\text{In}_2\text{O}_3$  would be greatly expanded if  $p$ -type conductivity could also be achieved [7, 8].

Most common dopants in  $\text{In}_2\text{O}_3$  act as donors, including hydrogen [9, 10]. This is explained by the relatively low position of the conduction band with respect to the vacuum level. A major difficulty in making  $\text{In}_2\text{O}_3$   $p$ -type is related to fundamental characteristics of its valence band [1, 11]. It is composed of O  $2p$  orbitals and lies very low in energy with respect to the vacuum level, so that all possible acceptor impurities lead to deep levels in the gap, with very high ionization energies [12]. Attempts to modify the electronic structure of wide-gap oxides to enable  $p$ -type doping have been proposed, yet with limited success [8, 13]. The key strategy has been to modify the top of the valence band by enhancing covalence through the orbital hybridization between O  $2p$  and metal cations [8, 13], or by incorporating isovalent anions, such as S and Se, with valence  $p$  orbitals that are higher in energy and more delocalized than the O  $2p$  [14, 15]. Building on recent ideas of using compounds containing post transition metals to modify the valence band [16–18], here we explore adding low concentrations of Bi to  $\text{In}_2\text{O}_3$ . We report on the stability, as well as the electronic structure and optical properties of  $(\text{In}_{1-x}\text{Bi}_x)_2\text{O}_3$  dilute alloys.

Bismuth belongs to the column 5A of the periodic table. In III-V semiconductors such as GaAs, InAs, and InSb, Bi substitute on the pnictide sites, acting as an isovalent pentavalent addition. However, Bi is also known to behave as a trivalent species, such as in  $\text{Bi}_2\text{Se}_3$  [19]

and  $\text{Bi}_2\text{O}_3$  [20, 21]. Considering the atomic size difference between In and O in  $\text{In}_2\text{O}_3$ , we expect that Bi will substitute on the In site.

Using density functional theory with a hybrid functional we calculate the electronic structure of dilute  $(\text{In}_{1-x}\text{Bi}_x)_2\text{O}_3$  alloys, with  $x=0.78\%$ ,  $3.13\%$ ,  $6.25\%$  and  $12.5\%$ . We find that Bi leads to an occupied band, composed of Bi  $s$  and O  $p$  orbitals, that is significantly higher in energy than the valence-band maximum (VBM) of the host material  $\text{In}_2\text{O}_3$ . The band gap, as well as the position and bandwidth of this new valence band can be tuned with Bi concentration (see Figure 1). Furthermore, this raised valence band in  $(\text{In}_{1-x}\text{Bi}_x)_2\text{O}_3$  dilute alloys not only leads to strong optical absorption in the visible spectral region, but also potentially enables  $p$ -type doping.

Our first-principles calculations are based on the density functional theory [22, 23] and the hybrid functional of Heyd-Scuseria-Ernzerhof (HSE06) [24, 25], as implemented in the VASP code [26, 27]. For the interaction between the valence electrons and the ionic cores, we used augmented plane wave (PAW) potentials [28, 29], with the following valence configurations: O( $2s^2 2p^4$ ), In( $4d^{10} 5s^2 5p^1$ ) and Bi( $5d^{10} 6s^2 6p^3$ ). The volume and atomic positions were relaxed using the semi-local exchange and correlation functional of Perdew, Burke, and Ernzerhof parameterized for solids (PBESol) [30], with an energy cutoff of 620 eV for the plane-wave expansion. For integrations over the Brillouin zone, we employed a  $3 \times 3 \times 3$   $\mathbf{k}$ -point mesh for the 40-atom primitive cell of bixbyite  $\text{In}_2\text{O}_3$ , and the same  $\mathbf{k}$ -points density for the other supercells.

Since PBE or PBESol drastically underestimate band gaps [24, 25, 31], we use the HSE06 to calculate the electronic structure of  $\text{In}_2\text{O}_3$  and  $(\text{In}_{1-x}\text{Bi}_x)_2\text{O}_3$  alloys. The HSE06 calculations were carried out for the crystal structures optimized with PBESol. In HSE06, the nonlocal Fock exchange is separated in short and long-

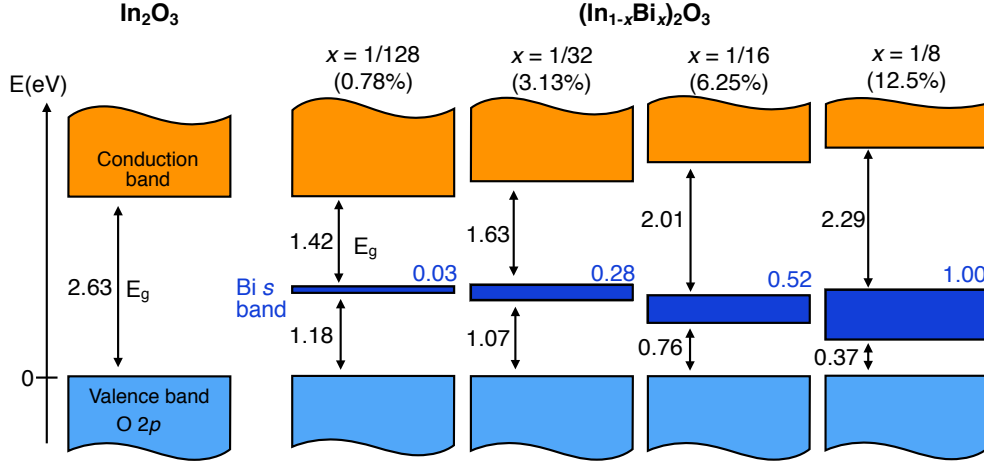


FIG. 1. Position of the valence and conduction bands in  $\text{In}_2\text{O}_3$  and dilute  $(\text{In}_{1-x}\text{Bi}_x)_2\text{O}_3$  alloys for Bi concentrations of  $x=1/128$  (0.78%),  $1/32$  (3.13%),  $1/16$  (6.25%), and  $1/8$  (12.5%). We used the valence-band maximum (VBM) of  $\text{In}_2\text{O}_3$  as reference and aligned the band edges of the alloys as described in the text. The band width of the Bi  $s$  band (valence band in the alloys) and the distance to the O  $2p$  bands are indicated.

range parts, by a screening function determined by the parameter  $\omega = 0.206$  [24, 25]. In the short-range region we used 25% of exact exchange, and 75% of PBE exchange, while the long range part is described by the PBE exchange [24, 25]. The electronic band structure and density of states were computed with a lower cutoff energy of 470 eV and a large  $7 \times 7 \times 7$   $\mathbf{k}$ -point mesh. For the optical properties we use the tetrahedral smearing method, but do not include excitonic effects due to the prohibitive computational cost.

$\text{In}_2\text{O}_3$  crystallizes in the body centered cubic bixbyite structure [32] with space group  $Ia\bar{3}$  and having 40 atoms (8 formula units) per primitive cell. All the O sites are equivalent, and each O atom is bonded to four In atoms, whereas each In atom is bonded to six O atoms. There are two inequivalent In octahedral sites, one forming a distorted octahedron, and the other forming a perfect octahedron (all In-O bond lengths are equal). Therefore, there are two possible sites for Bi to substitute for In in the bixbyite structure. We tested Bi substitution on both sites, and we find that Bi occupying the perfect octahedral site is only 12 meV lower in energy than the distorted site for  $(\text{In}_{1-x}\text{Bi}_x)_2\text{O}_3$  with  $x = 1/16$  (6.25%). The difference in the electronic structure of these two configurations is negligible, with band gaps differing by less than 10 meV. Therefore, we expect that Bi will incorporate on both perfect and distorted octahedral sites.

$(\text{In}_{1-x}\text{Bi}_x)_2\text{O}_3$  structures were built using one Bi in supercells of various sizes, from 40-atom to 320-atom, simulating dilute Bi concentrations of 0.78%, 3.13%, 6.25%, and 12.5%. We also tested using special quasi random structures (SQS) [33, 34] to simulate the alloys. The results were quite similar, with band gaps differing by less than 0.1 eV.

The calculated lattice parameter  $a_0$  and volume per

TABLE I. Calculated lattice parameter  $a_0$ , volume, and mixing enthalpy ( $\Delta H^f$ ) per cation of  $(\text{In}_{1-x}\text{Bi}_x)_2\text{O}_3$  alloys for various Bi concentrations ( $x$ ). For comparison, the experimental equilibrium lattice parameter of  $\text{In}_2\text{O}_3$  and volume per formula unit are 10.12 Å, and 64.78 Å<sup>3</sup> [32].

System	$x$ (%)	$\Delta H^f$ (meV/cation)	$a_0$ (Å)	Volume (Å <sup>3</sup> /f.u.)
$\text{In}_2\text{O}_3$	0	0	10.14	65.15
$(\text{In}_{1-x}\text{Bi}_x)_2\text{O}_3$	0.78	2	10.15	65.33
$(\text{In}_{1-x}\text{Bi}_x)_2\text{O}_3$	3.13	13	10.17	65.74
$(\text{In}_{1-x}\text{Bi}_x)_2\text{O}_3$	6.25	25	10.20	66.33
$(\text{In}_{1-x}\text{Bi}_x)_2\text{O}_3$	12.5	52	10.26	67.49

formula unit of  $\text{In}_2\text{O}_3$  and  $(\text{In}_{1-x}\text{Bi}_x)_2\text{O}_3$  alloys are listed in Table I. The calculated lattice parameter of 10.14 Å for  $\text{In}_2\text{O}_3$ , using PBEsol, is only 0.2% larger than the experimental value of 10.12 Å [32]. Adding Bi to  $\text{In}_2\text{O}_3$  leads to an increase in the lattice parameter since Bi has a larger atomic radius than In. We also calculated the mixing enthalpy for the  $(\text{In}_{1-x}\text{Bi}_x)_2\text{O}_3$  alloys, which we define as:

$$\Delta H^f = E_{\text{tot}}[(\text{In}_{1-x}\text{Bi}_x)_2\text{O}_3] - (1-x)E_{\text{tot}}(\text{In}_2\text{O}_3) - xE_{\text{tot}}(\text{Bi}_2\text{O}_3), \quad (1)$$

where  $E_{\text{tot}}[(\text{In}_{1-x}\text{Bi}_x)_2\text{O}_3]$  is the total energy of the alloy,  $E_{\text{tot}}(\text{In}_2\text{O}_3)$  is the total energy of  $\text{In}_2\text{O}_3$  and  $E_{\text{tot}}(\text{Bi}_2\text{O}_3)$  is the total energy of  $\text{Bi}_2\text{O}_3$  in its ground state. The calculated formation enthalpy of the  $(\text{In}_{1-x}\text{Bi}_x)_2\text{O}_3$  alloys are comparable to that found in  $(\text{Ga}_{1-x}\text{In}_x)_2\text{O}_3$  [35], which have been demonstrated experimentally [36]. For instance,  $\Delta H^f = 52$  meV/cation for  $(\text{In}_{1-x}\text{Bi}_x)_2\text{O}_3$  with  $x=12.5\%$ , whereas  $\Delta H^f = 50$  meV/cation for  $(\text{Ga}_{1-x}\text{In}_x)_2\text{O}_3$  for the same  $x$  [35]. Therefore, these

relatively low values of mixing enthalpies indicate that  $(\text{In}_{1-x}\text{Bi}_x)_2\text{O}_3$  alloys are likely to form.

The calculated electronic band structure and density of states (DOS) of  $\text{In}_2\text{O}_3$  and  $(\text{In}_{1-x}\text{Bi}_x)_2\text{O}_3$  alloy with  $x = 1/16$  and  $x = 1/8$  are shown in Figure 2. Note that, for  $x = 1/16$  an "ordered" structure was used to model the  $(\text{In}_{1-x}\text{Bi}_x)_2\text{O}_3$  alloy which maximize the Bi-Bi distance. In practice, we expect that random distribution of Bi would lead to a broadening of the band. Thus for  $x = 1/8$ , which Bi occupation was determined by SQS, we plot only the DOS.

The band structure and the DOS for  $\text{In}_2\text{O}_3$ , calculated using HSE06, shows a fundamental band gap of 2.63 eV, which is slightly lower than the previously reported value of 2.80 eV [1]. Adding Bi leads to a fully occupied band which is significantly higher in energy than the original VBM of the host  $\text{In}_2\text{O}_3$  material. This band originates from the coupling between the Bi  $s$  state, which is well below the VBM, with O  $2p$  states, mainly from the O atoms next to the Bi. Therefore, it has an antibonding character from the Bi  $s$  O  $p$  coupling. The minimum occurs at  $\Gamma$  and the maximum (VBM) occurs at the H point for the ordered alloy at  $x = 1/16$ . Note that, in a random alloy as it is modeled for  $(\text{In}_{1-x}\text{Bi}_x)_2\text{O}_3$  with  $x = 1/8$ , the plot of the density of states as shown in Fig. 2(c) is more relevant.

For the  $(\text{In}_{1-x}\text{Bi}_x)_2\text{O}_3$  alloy with  $x = 1/16$ , we find a band gap of 2.01 eV, with a new VBM about 1.28 eV higher than the VBM of  $\text{In}_2\text{O}_3$ . The band width of this higher valence band is 0.52 eV. The conduction-band minimum of the alloy, at  $\Gamma$ , is also pushed up by 0.66 eV, largely due to the interaction with the Bi  $s$  band. When the Bi concentration increase to  $x = 1/8$ , the band gap increased to 2.29 eV, with the antibonding Bi  $s$  band width of 1.00 eV and the CBM is pushed up by 1.03 eV.

The maximum of the O  $2p$  band in the  $(\text{In}_{1-x}\text{Bi}_x)_2\text{O}_3$  alloy occurs at approximately the same energy position as the VBM of the host  $\text{In}_2\text{O}_3$ , which is composed of O  $2p$ . The evolution of the band structure of the dilute  $(\text{In}_{1-x}\text{Bi}_x)_2\text{O}_3$  alloy with Bi concentration, shown in Figure 1, indicates that we can tune three key parameters in the  $(\text{In}_{1-x}\text{Bi}_x)_2\text{O}_3$  alloy by changing the Bi concentration: the positions of the valence-band (now derived from the antibonding Bi  $s$  state) and conduction-band edges, the band width of the valence band, and the band gap.

The repulsion between the Bi  $s$  valence band and the lowest energy conduction band also plays an important role in determining the band gap of the alloy. While the fundamental gap is direct at  $\Gamma$  in  $\text{In}_2\text{O}_3$ , it becomes indirect in the (ordered) alloy, with the VBM at H-point for  $x = 1/16$  and  $1/128$ , and at the R-point for  $x = 1/32$ . For the random alloys  $x = 1/8$ , the band gap has a pseudodirect nature.

We also calculated the absorption coefficient of dilute  $(\text{In}_{1-x}\text{Bi}_x)_2\text{O}_3$  alloys. Due to the high computational cost of calculating the optical properties of large sys-

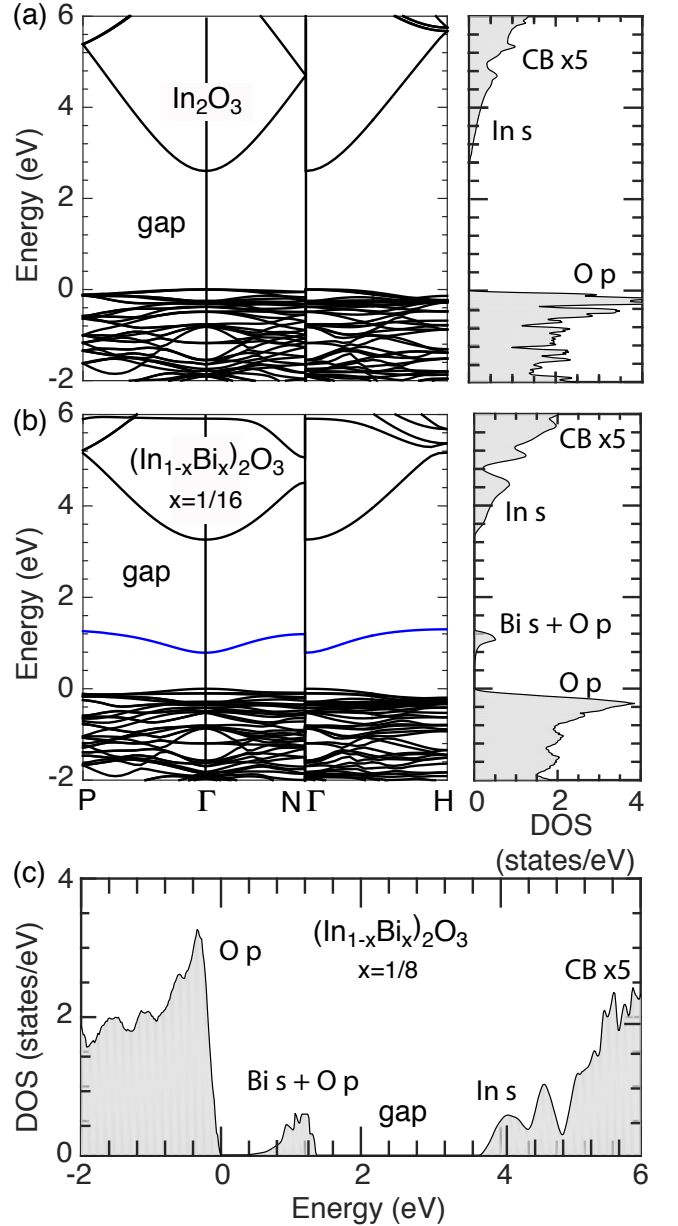


FIG. 2. Calculated band structure and density of states for (a)  $\text{In}_2\text{O}_3$  and (b)  $(\text{In}_{1-x}\text{Bi}_x)_2\text{O}_3$  with  $x=1/16$ , and (c)  $(\text{In}_{1-x}\text{Bi}_x)_2\text{O}_3$  with  $x=1/8$  aligned using the averaged electrostatic potential over a In atom in the bulk  $\text{In}_2\text{O}_3$  and in a In atom far from the Bi in the  $(\text{In}_{1-x}\text{Bi}_x)_2\text{O}_3$  alloy. The valence-band maximum (VBM) of  $\text{In}_2\text{O}_3$  was used as reference, and indicates that the VBM of the alloy is 1.28 eV ( $x=1/16$ ) and 1.37 eV ( $x=1/8$ ) higher than the original VBM of the host material.

tems with sufficient number of  $\mathbf{k}$ -points in HSE06, we performed these calculations using PBEsol and then applied a scissors operator to correct the fundamental band gap according to the HSE06 results. This approximation does not affect the lowest energy optical transitions, as tested using HSE06 and PBEsol for  $(\text{In}_{1-x}\text{Bi}_x)_2\text{O}_3$  with

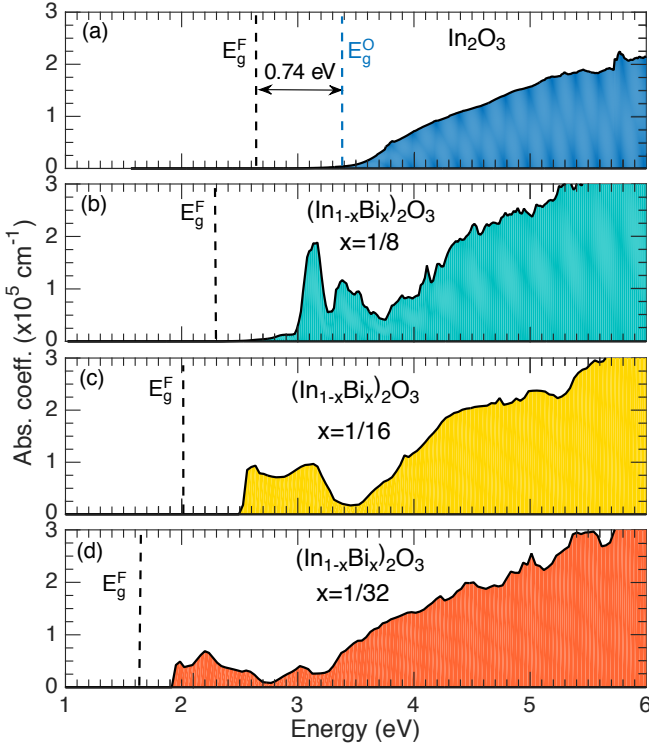


FIG. 3. Calculated absorption coefficient as a function of photon energy for  $\text{In}_2\text{O}_3$  and  $(\text{In}_{1-x}\text{Bi}_x)_2\text{O}_3$  with Bi concentrations  $x = 1/8$ ,  $x = 1/16$  and  $x = 1/32$ . The vertical dashed lines indicate the fundamental band gap ( $E_g^F$ ) and the optical band gap ( $E_g^O$ ). The disparity between  $E_g^F$  and  $E_g^O$  is also indicated.

$x = 1/16$ .

The optical properties of  $\text{In}_2\text{O}_3$  are well described in the literature, including the disparity between the optical and fundamental band gap [1, 11]. As shown in Figure 3(a), our results reproduce previous calculations for  $\text{In}_2\text{O}_3$ , where the optical absorption starts to increase only at photon energies that are 0.8 eV larger than the fundamental band gap  $E_g^F$ , defining the optical band gap  $E_g^O$ . Optical transitions with energy in the range from  $E_g^F$  to  $E_g^O$  have negligible contributions to the optical absorption coefficient, with magnitude smaller than  $1 \times 10^{-4}$  as indicated in Figure 3. This small contribution comes from the weak transitions from valence-band to conduction-band states at or in the vicinity of the  $\Gamma$  point [37].

As shown in Figure 3(b)-(d), we see a red shift in the onset of absorption of  $(\text{In}_{1-x}\text{Bi}_x)_2\text{O}_3$  alloys. This red shift decreases as the Bi concentration increases, consistent with the variation of the band gap with Bi concentration shown in Figure 1 and Figure 2. The peak associated with the transition from the antibonding Bi  $s$  valence band to the conduction band increases with the Bi concentration. We note, however, a seeming disparity between the optical and fundamental band gap in the

$(\text{In}_{1-x}\text{Bi}_x)_2\text{O}_3$  alloys, as shown in Figure 3(b)-(d). The origin of this disparity is associated to the indirect band gap in the alloys simulated using periodic supercells. In a real random alloy, the lack of long range order would lead to the collapse of the Brillouin zone to the  $\Gamma$  point, and the discussion of direct versus indirect band gap will lack meaning, so that we would expect transitions near or at the fundamental band gap to be allowed, but perhaps weak.

We note that the VBM in the  $(\text{In}_{1-x}\text{Bi}_x)_2\text{O}_3$  alloys is sufficiently higher in energy than the VBM in  $\text{In}_2\text{O}_3$  to allow for  $p$ -type doping. For example, introducing Mg dopants in  $\text{In}_2\text{O}_3$  leads to a deep acceptor level in the gap associated with the hole localized on an O atom next to the  $\text{Mg}_{\text{In}}$  substitutional impurity [12]. This acceptor level is about 0.9 eV above the VBM in  $\text{In}_2\text{O}_3$ . Therefore, in dilute  $(\text{In}_{1-x}\text{Bi}_x)_2\text{O}_3$  alloys, the same acceptor level is expected to appear close to the antibonding Bi- $s$ -derived VBM in the alloy (see band alignment in Figure 1), making it a shallow acceptor.

Finally, we believe our results can explain some puzzling results on  $\text{In}_2\text{O}_3$  samples containing Bi. A high intensity emission peak at 1.8 eV in the spectrum of nanocomposites of Bi-doped ITO has been reported by Na *et al.* [38]. The authors have attributed this emission to a transition from the conduction band to deep levels related to O vacancies. However, based on our results, for Bi concentration of approximately 1% in their experiments, the predicted optical band gap of the dilute  $(\text{In}_{1-x}\text{Bi}_x)_2\text{O}_3$  alloy is 1.8 eV, and a transition from conduction band to the antibonding Bi  $s$  band can explain this emission peak.

Considering the strong optical absorption in the visible spectrum of dilute  $(\text{In}_{1-x}\text{Bi}_x)_2\text{O}_3$  alloy, the conduction-band offset with  $\text{In}_2\text{O}_3$ , and the possibility of doping it  $p$ -type, we can think of  $(\text{In}_{1-x}\text{Bi}_x)_2\text{O}_3$  as a wide band gap absorption layer to be integrated in tandem solar cells where ITO is used as transparent contact. Note that there will be a tradeoff between band gap and the width of the antibonding Bi  $s$  valence band, which will have to be taken into consideration in the device design.

In summary, using electronic structure calculations, we show that incorporating low concentrations of Bi into  $\text{In}_2\text{O}_3$ , forming dilute  $(\text{In}_{1-x}\text{Bi}_x)_2\text{O}_3$  alloys, leads to significant changes in the electronic and optical properties of the parent compound, greatly extending its functionality. The Bi introduces an occupied intermediate valence band, composed mainly of Bi  $s$  and O  $p$ , resulting in significantly reduced band gaps. The position and band width of the new valence band in the  $(\text{In}_{1-x}\text{Bi}_x)_2\text{O}_3$  alloys can be tuned by controlling the Bi concentration. The high VBM of the  $(\text{In}_{1-x}\text{Bi}_x)_2\text{O}_3$  alloys can possibly enable  $p$ -type doping. The reduced band gap, compared to  $\text{In}_2\text{O}_3$  and strong near band edge absorption make dilute  $(\text{In}_{1-x}\text{Bi}_x)_2\text{O}_3$  alloys a promising wide-gap absorber layer in tandem solar cells.

# ACKNOWLEDGMENTS

This work at University of Delaware was supported by the National Science Foundation Faculty Early Career Development Program DMR-1652994. The work of SHW at CSRC was supported by the National Nature Science Foundation of China under Grant No. 11634003 and U1530401. This research was also supported by the the Extreme Science and Engineering Discovery Environment supercomputer facility, National Science Foundation grant number ACI-1053575, and the Information Technologies (IT) resources at the University of Delaware, specifically the high performance computing resources.

- 
- [1] A. Walsh, J. L. F. Da Silva, S. H. Wei, C. Körber, A. Klein, L. F. J. Piper, A. Demasi, K. E. Smith, G. Panaccione, P. Torelli, D. J. Payne, A. Bourlange, and R. G. Egdell, *Phys. Rev. Lett.* **100**, 167402 (2008).
  - [2] Z. Chen, W. Li, R. Li, Y. Zhang, G. Xu, and H. Cheng, *Langmuir* **29**, 13836 (2013).
  - [3] K. Nomura, H. Ohta, K. Ueda, T. Kamiya, M. Hirano, and H. Hosono, *Science* **300**, 1269 (2003).
  - [4] K. Nomura, H. Ohta, A. Takagi, T. Kamiya, M. Hirano, and H. Hosono, *Nature* **432**, 488 (2004).
  - [5] T. Minami, *Semicond. Sci. Technol.* **20**, S35 (2005).
  - [6] C. G. Granqvist, *Sol. Energy Mater. Sol. Cells* **91**, 1529 (2007).
  - [7] Y. Xu and M. A. Schoonen, *Am. Mineral.* **85**, 543 (2000).
  - [8] K. H. L. Zhang, K. Xi, M. G. Blamire, and R. G. Egdell, *J. Phys.: Condens. Matter* **28**, 383002 (2016).
  - [9] T. Koida, H. Fujiwara, and M. Kondo, *Jpn. J. Appl. Phys.* **46**, L685 (2007).
  - [10] T. Koida, M. Kondo, K. Tsutsumi, A. Sakaguchi, M. Suzuki, and H. Fujiwara, *J. Appl. Phys.* **107**, 033514 (2010).
  - [11] F. P. Sabino, R. Besse, L. N. Oliveira, S.-H. Wei, and J. L. F. Da Silva, *Phys. Rev. B* **92**, 205308 (2015).
  - [12] S. Lany and A. Zunger, *Phys. Rev. B* **80**, 085202 (2009).
  - [13] H. Kawazoe, M. Yasukawa, H. Hyodo, M. Kurita, H. Yanagi, and H. Hosono, *Nature* **389**, 939 (1997).
  - [14] H. Hiramatsu, K. Ueda, H. Ohta, M. Orita, M. Hirano, and H. Hosono, *Thin Solid Films* **411**, 125 (2002).
  - [15] H. Hiramatsu, K. Ueda, H. Ohta, M. Hirano, M. Kikuchi, H. Yanagi, T. Kamiya, and H. Hosono, *Appl. Phys. Lett.* **91**, 012104 (2007).
  - [16] Y. Ogo, H. Hiramatsu, K. Nomura, H. Yanagi, T. Kamiya, M. Kimura, M. Hirano, and H. Hosono, *Phys. Status Solidi A* **206**, 2187 (2009).
  - [17] H. Yabuta, N. Kaji, R. Hayashi, H. Kumomi, K. Nomura, T. Kamiya, M. Hirano, and H. Hosono, *Appl. Phys. Lett.* **97**, 072111 (2010).
  - [18] A. Bhatia, G. Hautier, T. Nilgianskul, A. Miglio, J. Sun, H. J. Kim, K. H. Kim, S. Chen, G.-M. Rignanese, X. Gonze, and J. Suntivich, *Chem. Mater.* **28**, 30 (2016).
  - [19] P. Shuk, H.-D. Wiemhfer, U. Guth, W. Gpel, and M. Greenblatt, *Solid State Ionics* **89**, 179 (1996).
  - [20] A. Walsh, G. W. Watson, D. J. Payne, R. G. Egdell, J. Guo, P.-A. Glans, T. Learmonth, and K. E. Smith, *Phys. Rev. B* **73**, 235104 (2006).
  - [21] A. Matsumoto, Y. Koyama, and I. Tanaka, *Phys. Rev. B* **81**, 094117 (2010).
  - [22] P. Hohenberg and W. Kohn, *Phys. Rev.* **136**, B864 (1964).
  - [23] W. Kohn and L. J. Sham, *Phys. Rev.* **140**, A1133 (1965).
  - [24] J. Heyd and G. E. Scuseria, *J. Chem. Phys.* **120**, 7274 (2004).
  - [25] J. Heyd, G. E. Scuseria, and M. Ernzerhof, *J. Chem. Phys.* **124**, 219906 (2006).
  - [26] G. Kresse and J. Hafner, *Phys. Rev. B* **48**, 13115 (1993).
  - [27] G. Kresse and J. Furthmüller, *Phys. Rev. B* **54**, 11169 (1996).
  - [28] P. E. Blöchl, *Phys. Rev. B* **50**, 17953 (1994).
  - [29] G. Kresse, *Phys. Rev. B* **59**, 1758 (1999).
  - [30] J. P. Perdew, A. Ruzsinszky, G. I. Csonka, O. A. Vydrov, G. E. Scuseria, L. A. Constantin, X. L. Zhou, and K. Burke, *Phys. Rev. Lett.* **100**, 136406 (2008).
  - [31] J. P. Perdew, *Int. J. Quantum Chem.* **28**, 497 (1985).
  - [32] M. Marezio, *Acta Cryst.* **20**, 723 (1966).
  - [33] A. Zunger, S.-H. Wei, L. G. Ferreira, and J. E. Bernard, *Phys. Rev. Lett.* **65**, 353 (1990).
  - [34] S.-H. Wei, L. G. Ferreira, J. E. Bernard, and A. Zunger, *Phys. Rev. B* **42**, 9622 (1990).
  - [35] H. Peelaers, D. Steiauf, J. B. Varley, A. Janotti, and C. G. Van de Walle, *Phys. Rev. B* **92**, 085206 (2015).
  - [36] M. Baldini, D. Gogova, K. Irmscher, M. Schmidbauer, G. Wagner, and R. Fornari, *Cryst. Res. Technol.* **49**, 552 (2014).
  - [37] F. P. Sabino, L. N. Oliveira, S.-H. Wei, and J. L. F. Da Silva, *J. Phys.: Condens. Matter* **29**, 085501 (2017).
  - [38] H. G. Na, T.-K. Jung, J.-W. Lee, S.-K. Hyun, Y. J. Kwon, A. Mirzaei, T.-B. Kim, Y.-C. Shin, H.-J. Choi, H. W. Kim, and C. Jin, *Mater. Res. Express* **3**, 095016 (2016).